CEBAF Program Advisory Committee Ten Proposal Cover Sheet

This document must be received by close of business on Tuesday, December 19, 1995 at:

CEBAF
User Liaison Office, Mail Stop 12 B
12000 Jefferson Avenue
Newport News, VA 23606

(Choose one)

☒ **New Proposal Title:** Measurement of K° Electroproduction

☐ **Update Experiment Number:**

☐ **Letter-of-Intent Title:**

Contact Person

Name: Richard A. Magahiz

Institution: Carnegie Mellon University

Address: Department of Physics, Wean Hall

Address:

City, State ZIP/Country: Pittsburgh, PA 15213 USA

Phone: (412) 268 - 0949 **FAX:** (412) 681 - 0648

E-Mail → Internet: magahiz@ernest.phys.cmu.edu
http://www.phys.cmu.edu/hyperons/homepage.html

Experimental Hall: B **Days Requested for Approval:** 0 (additional)

CEBAF Use Only

Receipt Date: 12/19/95 PR 95-003

By: gp

PROPOSAL to the CEBAF Program Advisory Committee

Measurement of K° Electroproduction

R. A. Magahiz (Spokesperson), A. Berdoz, D. S. Carman, G. B. Franklin, C. A. Meyer,

R. A. Schumacher, B. P. Quinn

Department of Physics, Carnegie Mellon University, Pittsburgh, PA

K. S. Dhuga, C. Bennhold, W. J. Briscoe, H. Ito

Center for Nuclear Studies, George Washington University, Washington, DC

M. Anghinolfi, P. Corvisiero, G. Ricco, M. Ripani, M. Taiuti, S. Zucchiatti

Instituto Nazionali di Fisica Nucleare, Genova, Italy

J. Mueller

Department of Physics, University of Pittsburgh, Pittsburgh, PA

M. D. Mestayer

Physics Division, CEBAF, Newport News, VA

C. R. Münz

Institut für Theoretische Kernphysik, Universität Bonn, 53115 Bonn, Germany

T. Mart

Institut für Kernphysik, Universität Mainz, D55099 Mainz, Germany

S. Cotanch

North Carolina State University, Raleigh, NC

W. W. Buck, R. A. Williams

Department of Physics, Hampton University, Hampton, VA, and CEBAF, Newport News, VA

and the **CLAS Collaboration**

(December 18, 1995)

Contents

Abstract

The reaction $p(e, e'K^\circ)\Sigma^+$ can play an important role in our understanding of the mechanism of the electromagnetic production of strangeness, since it would provide complementary information to that given by charged kaon electroproduction and by charged and neutral kaon photoproduction. The CLAS Large Acceptance Spectrometer provides a unique means to observe this process for the first time through the two-pion decay modes of the K°. K° events will be identified through reconstruction of the invariant mass of the pion pairs and the missing mass of the undetected hyperon. Simulations show that a cut to identify K° decay tracks which are well separated from the electron vertex will make it possible to reduce multipion background further. By measuring the cross section as a function of Q^2, we can test specific predictions of recent theoretical models for the $K^{*\circ}K^\circ\gamma$ transition form factor, which enters in through the dominant t-channel diagram.

I. STRANGENESS PRODUCTION AT CEBAF

There has been a great deal of interest recently in charged kaon electroproduction as a means of testing theoretical models of strangeness production [1–5]. The goals are to better determine the basic electromagnetic couplings of the nucleon and to gain insight into the reaction mechanism of strangeness production. The electromagnetic production of the neutral kaon will serve as an additional probe to broaden our knowledge of strangeness degrees of freedom in hadrons. The additional isospin channels accessed through K° production are complimentary to the K^+ data, but to obtain this information significant additional analysis will be needed, which we believe calls for this separate proposal. Also, new information not available via K^+ production will be obtained.

Only two published reports of the photoproduction of K° exist, (Figures 1 and 2) with very poor statistics. [6] No data at all are reported in the literature on the electroproduction of K° at moderate energies, owing to the near impossibility of measuring multiple particles in the final state using one- or two-arm spectrometers. We lack even the most basic information about the cross section, the important resonant channels, and the dependence on the four-momentum transfer, and can only use indirect methods to estimate what to expect at CEBAF. Observation of $p(e,e'K^\circ)\Sigma^+$ at CEBAF would fill this gap in our understanding of the electromagnetic production of strangeness.

The transition form factor $F_{K^\circ K\gamma}$ would be an interesting quantity to study not only because of its role in strangeness production, but also because of the analogy with the non-strange transition form factor $F_{\rho\pi\gamma}$ which theories have sought to understand for some time. Just as the transition form factors of baryon resonances will tell us about the internal structure of the nucleon, this mesonic transition form factor would clarify what the best picture of the kaon would be at intermediate energies. We will describe how the different theories lead to very different predictions about the Q^2 behavior of the cross section for K° electroproduction.

II. THEORETICAL CONSIDERATIONS

A. Overview

Until fairly recently, the only models of kaon electroproduction used a quantum hadrodynamic (QHD) framework seeking to describe the basic process in terms of a selected number of tree level s, t, and u channel diagrams (Figure 3). The states which appear in diagrams represent poles in the complex energy plane, describing effective degrees of freedom of the underlying field theory. The output from the fits to existing data [7] is a set of coupling constants which may be compared to SU(3) predictions. For the charged kaon case, both Λ and Σ° hyperons appear in the final state and are respresented by two different phenomenological coupling constants. The calculations differ in the selection of meson and baryon resonances considered, the treatment of the electromagnetic form factors and final state interactions [2], and the incorporation of duality and crossing symmetries. [3]

Work is underway on extending the models to the case of K° electroproduction where there is no data. Part of the interest is that the absence of Λ in the final state changes the character of the diagrams which contribute [8], which is to say the resonance structure will be quite different. The uncertainties in estimation of the model parameters are greatly reduced if one is in a position to include data for both charged and neutral kaon electroproduction. Also, in the t channel, the lightest meson which can contribute a Born term diagram at $Q^2 = 0$ is the $K^{*\circ}$, unlike the charged kaon case where the Born diagram featuring a virtual K^+ is allowed. It is here where this experiment will have the biggest impact.

In the last two years there has been a flurry of papers adopting a relativistic constituent quark picture to understand kaon electroproduction and photoproduction. [9] In general, the quark models show much promise for describing the electroproduction of strange particles with fewer parameters than the phenomenological models, and possibilities for relating features of the calculations to the actual physics. The predictions of these models

for the kaon form factors vary widely, stimulating interest in a proposal to measure the kaon form factor using a deuterium target. [10] In this proposal, we shall investigate the results of one calculation [11] which has specific predictions for the $K^{*\circ}K^{\circ}\gamma$ transition form factor, comparing it to a QHD model. [4]

B. Transition form factors

The dominant t-channel Born term in K° electroproduction for small Q^2 is virtual $K^{*\circ}$ exchange. It involves the same electromagnetic vertex responsible for the radiative decay of the $K^{*\circ}$, with the added feature that the vector meson is far off-shell. The Q^2 dependence of this coupling can be described by a transition form factor which may be calculated in a covariant quark model [11], a spectral model using dispersion theory [12], or using naive vector dominance. (See Figure 4.) The different treatments show different magnitudes and asymptotic behavior.

Figure 5 shows the effect of two of the forms of the transition form factor on the differential cross section, as calculated in a QHD framework. The "no form factor" curve shows how the model behaves in a nonphysical way at higher values of Q^2, while the other two curves show a more reasonable asymptotic behavior when a transition form factor derived from a vector dominance model [4] or one from the covariant quark model is inserted. In all cases, the cross section was calculated at a single hadronic center of mass kaon angle (100 degrees from the virtual photon direction). The quark model calculation reduces the cross section the most at higher values of Q^2. In addition, the model predicts a W dependence rising up smoothly from threshold. It seems clear that high-precision data on the $K^{\circ}\Sigma^{+}$ channel from CEBAF will greatly improve our ability to choose among these and other models.

C. Longitudinal and transverse amplitudes

The complete lack of data in K° electroproduction makes the measurement of the differential cross section as a function of Q^2 and W a matter of primary importance for the proposed experiment described here. Although we are concentrating on the cross section here as an indirect probe of the $K^{*\circ}K^\circ\gamma$ transition form factor, we would like to mention one additional piece of information we would expect to gain in addition which should shed some light on the current models of strangeness production.

We have performed an extensive feasibility study of a measurement of the longitudinal and transverse amplitudes σ_T and σ_L via a Rosenbluth-type separation of the differential cross section. The general formula for the $(e, e'X)$ process is:

$$\frac{d\sigma}{d\Omega} = \sigma_T + \epsilon\sigma_L + \epsilon\sigma_{TT}\cos 2\phi + \sqrt{\epsilon(\epsilon+1)}\sigma_{LT}\cos\phi$$

where ϵ is the virtual photon polarization parameter. The theoretical interest lies in the comparison of the amplitudes between the charged [5] and neutral kaon cases as an additional piece of experimental information to constrain theory. We find that if one pays proper attention to understanding all the possible sources of systematic errors, the statistics should be adequate to impose meaningful limits on current theories when combined with the analogous charged kaon L-T separation results.

D. Background due to multipion electroproduction

Figure 6 shows the relative cross sections for different exclusive channels. [13] If we compare the photoproduction cross sections for the $n\pi^+\pi^+\pi^-$ and $p\pi^\circ\pi^+\pi^-$ backgrounds in this figure to those measured for K° photoproduction (Figure 2), we see that the electroproduction experiment must be able to reduce over an order of magnitude of background. We plan to reject multipion events through cuts on the $\pi^+\pi^-$ invariant mass, missing mass of the Σ^+, and kaon decay vertex position relative to the electron vertex. In the next few sections we will give reasons to be optimistic that such measures can in fact reduce the

background enough to allow us to make an accurate measurement of the Q^2 distribution of the K° signal.

III. EXPERIMENTAL CONSIDERATIONS

In the following sections, we shall describe the experimental requirements of the K° electroproduction measurement and results of simulations of the expected performance of the CEBAF Large Acceptance Spectrometer (CLAS). For simplicity, we have taken the approach of simulating our signal K° events by an isotropic angular distribution in the hadronic center of mass frame, with K° and Σ^+ decays also generated isotropically in their own rest frames. To estimate the background, we have employed the CELEG event generator [14] that uses empirical cross sections, masses, and widths to simulate hadron electroproduction. In either case, to simulate the performance of CLAS we passed the generated events through the parametric Monte Carlo simulation program FASTMC [15] which reproduces the overall resolution, acceptance, and particle identification capability of the detector without the detailed tracking of a full detector simulation such as GEANT. In our simulations, we have chosen a magnetic field that bends negative particles in toward the beam axis. The plots comparing signal to background distributions have all been generated assuming a total virtual photon cross section into $K^\circ\Sigma^+$ of 50 nb, simply scaling one estimate [5] for the cross section into $K^+(\Lambda, \Sigma^\circ)$ by the ratio of the photoproduction cross sections (Figure 2). In future studies, we expect to model the physics in fuller detail using more elaborate event generators and detector simulation packages.

A. CLAS capabilities summarized

The CLAS [16] is a toroidal magnetic spectrometer designed to enable experiments which demand good acceptance for coincident detection of multiple particles in the hadronic final state. Three sets of drift chambers provide tracking with good momentum

and angular resolution for charged particles, gas Čerenkov detectors and time of flight counters provide particle identification, and electromagnetic shower counters provide sensitivity to neutrals such as gammas and neutrons. (Figure 7)

1. Electron identification

To cover the entire range in Q^2 and ϵ, one needs to detect and identify electrons over a wide range of scattering angles. For angles less than 45°, the gas Čerenkov counters are expected to be at least 99% efficient for electrons over their geometric acceptance [17], providing excellent $\pi - e$ separation.

2. Charged particle tracking and acceptance

In electron scattering with a known beam energy on a proton target, the quantities Q^2 and W are determined fully by measuring the scattering angle and momentum of the outgoing electron. The tracking chambers of CLAS are designed to reconstruct particle trajectories through the toroidal magnetic field. Errors in momentum determination come from chamber resolution, multiple scattering, and dE/dx. Figure 8 shows the simulated momentum error for tracking 2.21 GeV/c electrons at 20° through the drift chambers. The rms of the distribution is 2.7 MeV/c, giving a FWHM resolution of better than 0.5%. At larger polar angles and at lower settings of the overall magnetic field, the momentum resolution is not as good because of the smaller value of $\int B \cdot dl$. Our simulation takes this into account.

The dominant limitations to accurate measurement of Q^2 will probably be the systematic errors such as absolute calibration of the electron beam energy, acceptance of the spectrometer, calibration of particle angles, and radiative corrections. To minimize systematic momentum errors, the drift chambers will undergo an extended period of alignment relative to one another and to the target position, using survey measurements, cosmic rays, angle-defining slits, and overconstrained reactions.

Our preliminary study (section III A 4) reveals that there are still some poorly understood aspects of the particle acceptance for tracks with do not start at the electron vertex. We find that the pattern recognition requirements to deal with such tracks can in some cases be quite different from those needed for tracking the prompt charged tracks which make up the bulk of the data we expect from CLAS. These requirements are similar to what we expect to encounter during real photon running with extended targets, and it is clear that careful software development to meet the demands will be a high priority item as we prepare for detector commissioning. For the present investigation of K° electroproduction to succeed, therefore, we will need to pay close attention to the way we develop the data reduction software so that detached track candidates will not be lost before final analysis.

3. Invariant mass resolution

Figure 9 shows the distribution in invariant mass for $\pi^+\pi^-$ from K°_S decay accepted into CLAS. Compare the peak to the data shown in Figure 1, which has a width ten times larger. We propose to take advantage of this sharp peak as our primary cut to distinguish K° electroproduction from the incoherent background.

Figure 10a shows the missing mass distribution for both signal events and background $(e, e'\pi^+\pi^-)$ events with no cut imposed on the reconstructed K° mass. In Figure 10b, we give the same comparison for events selected with an additional cut on the K° mass. The Σ^+ missing mass distribution is clearly separated from background. Because this background study does not yet include much of the actual physics of multiparticle production (such as correlations) and because it is still limited in statistics, the encouraging results so far should be regarded as simply suggestive of the effectiveness of this primary cut on data.

4. Detached vertex identification

The clearest signature of K°_S production would be the observation of the $\pi^+\pi^-$ vertex spatially displaced from the line of the outgoing electron track. This relies not only on minimizing the amount of multiple scattering in the target and through the detector, but also on accurate information of the position of the innermost Region 1 drift chamber. Precise coordinate measurements of the wire positioning elements of Region 1 suggest that individual drift cell positions can be known to an accuracy of 125 μm [18].

Conceptually, the detached vertex identification algorithm can be separated into four parts: (1) Identification of particle tracks which are spatially separate from the electron vertex. (2) Invariant mass reconstruction of the K° from the two pions to reject background. (3) Construction of the K° decay vertex from the point of closest approach of the pion tracks. (4) Refinement of K° kinematics by constrained fit of the the decay pion tracks to the vertex position. Experience with K°_S vertex finding algorithms at CLEO and at CDF suggest that this process can improve the momentum measurement of the kaon by a large degree over a simple one-pass track fit through the tracking chambers.

We have studied the performance of the SDA tracking code with simulated tracks displaced from the primary vertex to estimate how well we might be able to identify detached vertices in CLAS. To distinguish between tracks pointing to the vertex and detached tracks, we computed the *impact parameter*, defined as the perpendicular distance between the nominal target position and the extrapolation of the track back toward the target. We studied two aspects of the problem as a function of impact parameter: (1) the spatial resolution of the tracking for particles (Figure 11), and (2) the efficiency of the code for finding tracks which do not point back at the target (Figure 12). The first of these is important in determining how small a cut we can make on the K° vertex separation from the electron track. The second plays a large role in determining the acceptance of the spectrometer for kaons which decay far from the target. Our simulation shows that the impact parameter is a useful variable to use as a first pass cut to identify candidate K°_S decay pions.

Based on the distribution of decay pion track momenta and impact parameters (Figure 13) we chose a minimum impact parameter cut of 0.9 cm (3σ) and a maximum cut of 8.0 cm on pion tracks. This gave a fairly respectable K^0_S detection efficiency η_{vtx} of about 40% for all beam energies. More simulation is required to optimize the cuts for the best background rejection.

B. Estimate of acceptance

Our simulation requires the following:

1. that the scattered electron be identified by the gas Čerenkov detectors,

2. that the π^+ reach the scintillation counters,

3. that the π^- be tracked through all three regions of drift chambers,

4. that the pions pass the impact parameter cut described above.

(See Figure 7 for an event picture showing three longitudinal sections through CLAS.)

Table I gives η_e, the efficiency of detecting electrons for various values for the beam energies, Q^2, and W. This varies smoothly with Q^2 and W, as seen in the comparison of the curves in Figure 14. As either Q^2 or W increases, so does the electron angle, affecting the azimuthal acceptance of CLAS. At electron angles greater than about 45°, the requirement that the electron hit the one sector instrumented with the large angle shower calorimeter cuts the acceptance by a factor of about six. Table II gives $\eta_{K^0|e}$, the efficiency of detecting a $\pi^+\pi^-$ pair once the electron has been accepted. As W increases, the kaon momentum increases, making it more likely that the π^- from its decay make it through the spectrometer instead of going into the forward hole.

Table III gives the plan for allocation of approved beam time using a high-pressure hydrogen gas target in Hall B, as outlined by the N^* collaboration. The bulk of the time is allocated at the beam energy of 4.0 GeV/c, at full magnetic field, with lower energy

runs to be taken with reduced field to increase forward particle acceptance. This reduction of the magnetic field clearly increases the kaon detection efficiency in our range of interest. The luminosity limit is basically set by the rate the inner drift chamber can withstand; the design of the Region 1 drift chamber was carried out with this in mind. Table IV takes the beam time numbers, the CLAS acceptance, and the virtual photon flux factor Γ_T to calculate total numbers of events. The rate formula is as follows:

$$\text{Rate} = \mathcal{L} \cdot \Gamma_T \cdot \sigma(Q^2, W) \cdot \Delta Q^2 \cdot \Delta W \cdot \eta_e \cdot \eta_{K^\circ|_e} \cdot \eta_{vtx} \cdot B(K^\circ \rightarrow \pi^+\pi^-)$$

where Γ_T is the viritual photon flux, ΔQ^2 and ΔW are bin widths, and B is the branching ratio to two charged pions. In the rate calculation we corrected the cross section given by the model described in section II B for the variation in acceptance over kaon angle in the hadronic center of mass.

Figure 15 shows the expected Q^2 distribution expected under the two models for the transition form factor. The width of the curves indicated the statistical error bars; the irregularities in the curves reflect the finite statistics of the simulations. We see that the two models predict very different event totals and Q^2 distributions, well beyond the statistical uncertainties of our measurement.

IV. CONCLUDING REMARKS

We believe that the current theoretical interest in measuring the electromagnetic form factor of pseudoscalar mesons leads naturally to the idea of measuring K° electroproduction for the first time ever. Experimentally, we feel that cuts on the invariant kaon mass and on the impact parameter of pion tracks will enable us to make an accurate measurement of the Q^2 distribution of this process. Theoretical calculations of the cross section tell us that this would set significant limits on the $K^{*\circ}K^\circ\gamma$ transition form factor. Additionally, the information we expect to gain on the longitudinal and transverse form factors in K° electroproduction will be of great interest when combined with the results of

the charged kaon electroproduction experiments. This K° electroproduction program would be consitstent with the approved experiments in CLAS in terms of trigger configuration, magnetic field configuration, and target design. Our investigations have already stimulated detailed study of the software requirements for efficient detached track detection in the CLAS reconstruction software, and we expect that the proposed experiment will benefit the experimental program as a whole in many other ways.

1. P. Markowitz, Workshop on CEBAF at Higher Energies, April 1994, 353-358. O. K. Baker, Workshop on CEBAF at Higher Energies, April 1994, 191-195.
2. C. Bennhold, Nucl. Phys. A547 (1992) 79c-88c.
3. S.R. Cotanch, R.A. Williams, and C.R. Ji, Phys. Scr. 48 (1993) 217-225.
4. R. A. Williams, C. R. Ji, and S. R. Cotanch, Phys. Rev. C 46(1992) 1617-165.
5. O. K. Baker, *et al.*, CEBAF Proposal 93-018. M. D. Mestayer, K. H. Hicks, *et al.*, CEBAF Proposal 93-030.
6. D. P. Barber, *et al.*, Nucl. Inst. and Meth. 155 (1978) 353-369. Aachen-Bonn-Hamburg-Heidelberg-München collaboration, R. Erbe *et al.*, Phys. Rev. 188 (1969) 2060.
7. T. Azemoon, *et al.*, Nucl. Phys. B95 (1975) 77-97. C. J. Bebek, *et al.*, Phys. Rev. D15 (1977) 3082-3084. C. T. Day, *et al.*, Phys. Rev. D23 (1981) 576-586.
8. T. Mart, C. Bennhold, C. E. Hyde-Wright, Phys. Rev. C51 (1995) R1074.
9. A. Szczepaniak, C. R. Ji, and S. R. Cotanch, North Carolina State University preprint HEP-PH/9309282. F. Schlumpf, Phys. Rev. D50 (1994) 6895-6898. F. Cardarelli *et al.*, preprint NUCL-TH/9507038. Z. Li, preprint HEP-PH/9502218. Buck, W. W., Williams, R. A., and Ito, H., Phys. Lett. B 351 (1995) 24.
10. K. Dhuga, private communication.
11. C. R. Münz, J. Resag, B. C. Metsch, H. R. Petry, Phys. Rev. C52 (1995) 2110.
12. R. A. Williams, private communication.
13. M. Ripani, *et al.*, CEBAF Proposal 93-006.

14. D. Joyce, CEBAF, CLAS-NOTE 89-004. Our implementation includes excitation of $\Delta(1232)$, $\Delta(1620)$, $\Delta(1700)$, $\Delta(1900)$, $\Delta(1905)$, $\Delta(1910)$, $\Delta(1920)$, $\Delta(1930)$, $\Delta(1950)$, $N^*(1440)$, $N^*(1520)$, $N^*(1535)$, $N^*(1650)$, $N^*(1675)$, $N^*(1680)$, $N^*(1700)$, $N^*(1710)$, and $N^*(1720)$ resonances, $\rho(770)$ production, and deep inelastic processes.
15. E. Smith, CEBAF, CLAS-NOTE 90-003.
16. CEBAF Hall B Conceptual Design Report, April 1990.
17. E. A. Doroshkevich, A. V. Vlassov, and M. V. Kossov, CEBAF, CLAS-NOTE 94-006.
18. R. A Schumacher. and R. Magahiz, Carnegie Mellon, CLAS-NOTE 94-018.

List of figures

TABLES

E_0	2.4			2.8			3.2				4.0			
Q^2	0.5	1.0	1.5	0.5	1.0	1.5	0.5	1.0	1.5	2.0	1.0	1.5	2.0	2.5
W=1.8	0.72	0.75	0.13	0.61	0.73	0.75	0.53	0.68	0.76	0.75	0.57	0.64	0.70	0.25
W=2.0	0.75	0.47	0.00	0.69	0.47	0.00	0.59	0.72	0.75	0.00	0.69	0.69	0.74	0.00
W=2.2	0.00	0.00	0.00	0.68	0.33	0.00	0.65	0.00	0.00	0.00	0.63	0.71	0.75	0.00
W=2.4	0.00	0.00	0.00	0.00	0.00	0.00	0.65	0.00	0.00	0.00	0.69	0.00	0.00	0.00

TABLE I. Electron acceptance for various values of E_0, Q^2, and W

E_0	2.4			2.8			3.2				4.0			
Q^2	0.5	1.0	1.5	0.5	1.0	1.5	0.5	1.0	1.5	2.0	1.0	1.5	2.0	2.5
W=1.8	0.33	0.28	0.23	0.33	0.28	0.26	0.34	0.30	0.26	0.22	0.15	0.13	0.11	0.09
W=2.0	0.33	0.32	0.00	0.33	0.32	0.28	0.33	0.32	0.32	0.26	0.17	0.17	0.15	0.13
W=2.2	0.00	0.00	0.00	0.34	0.32	0.00	0.35	0.32	0.30	0.00	0.21	0.19	0.17	0.00
W=2.4	0.00	0.00	0.00	0.00	0.00	0.00	0.35	0.00	0.00	0.00	0.23	0.00	0.00	0.00

TABLE II. K° acceptance for events where electron is accepted

Energy (GeV)	B/B_o	Hours	Luminosity $\mathcal{L}$ $(10^{33} cm^{-2} s^{-1})$
2.4	0.5	250	5
2.8	0.5	96	10
3.2	0.5	96	10
4.0	1.0	800	10

TABLE III. CLAS N^* run plan on hydrogen targets.

VMD transition form factor															
E_0	2.4			2.8			3.2				4.0				
Q^2	0.5	1.0	1.5	0.5	1.0	1.5	0.5	1.0	1.5	2.0	1.0	1.5	2.0	2.5	
W=1.8	66100	13100	700	43800	9600	3300	38600	9300	1200	0	11400	3900	1500	200	
W=2.0	158400	24000	0	109500	17600	0	93200	26300	10200	0	37400	13700	15900	0	
W=2.2	0	0	0	145300	17100	0	140000	0	0	0	54000	21800	10400	0	
W=2.4	0	0	0	0	0	0	162700	0	0	0	75600	0	0	0	
Total	262000			346000			484000				236000				

Bonn transition form factor															
E_0	2.4			2.8			3.2				4.0				
Q^2	0.5	1.0	1.5	0.5	1.0	1.5	0.5	1.0	1.5	2.0	1.0	1.5	2.0	2.5	
W=1.8	34400	4000	100	23000	2900	600	22100	3100	700	200	3700	800	200	0	
W=2.0	82400	7200	0	57400	5300	0	53300	8700	2100	0	12000	2800	800	0	
W=2.2	0	0	0	76100	5200	0	79800	0	0	0	17300	4400	1400	0	
W=2.4	0	0	0	0	0	0	93000	0	0	0	24200	0	0	0	
Total	128000			171000			263000				67000				

TABLE IV. Estimate of total number of events.

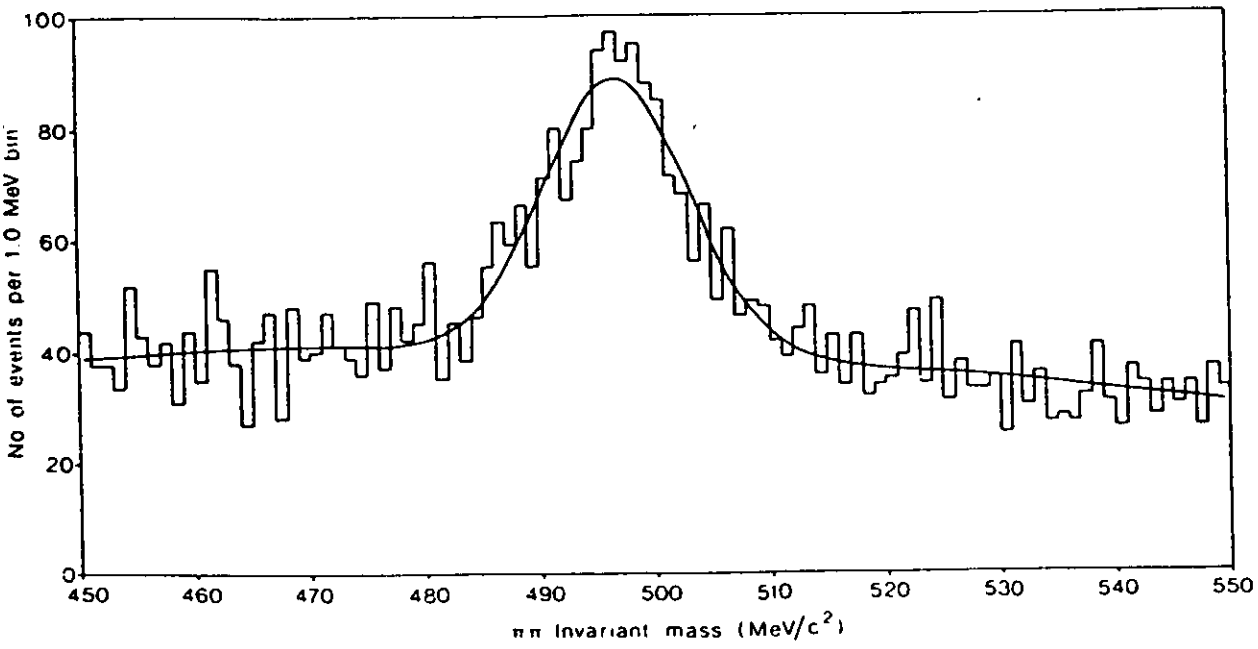

FIG. 1. Photoproduced K_S° peak in $\pi^+\pi^-$ measured by LAMP2 collaboration.

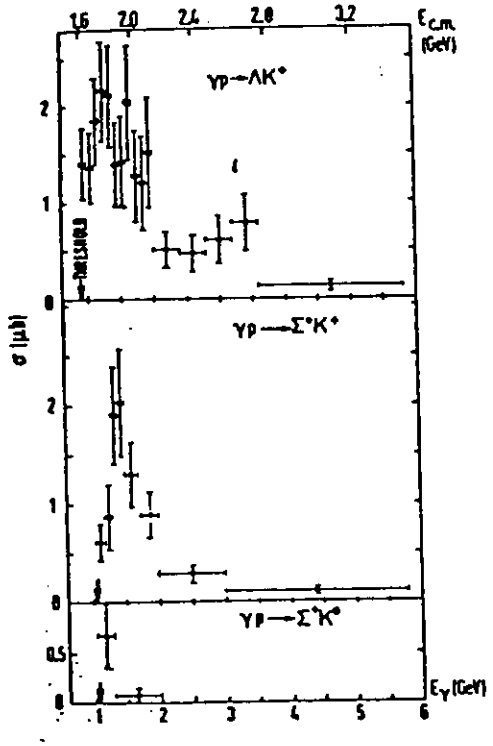

FIG. 2. K_S° photoproduction cross section measured by Erbe *et al.*

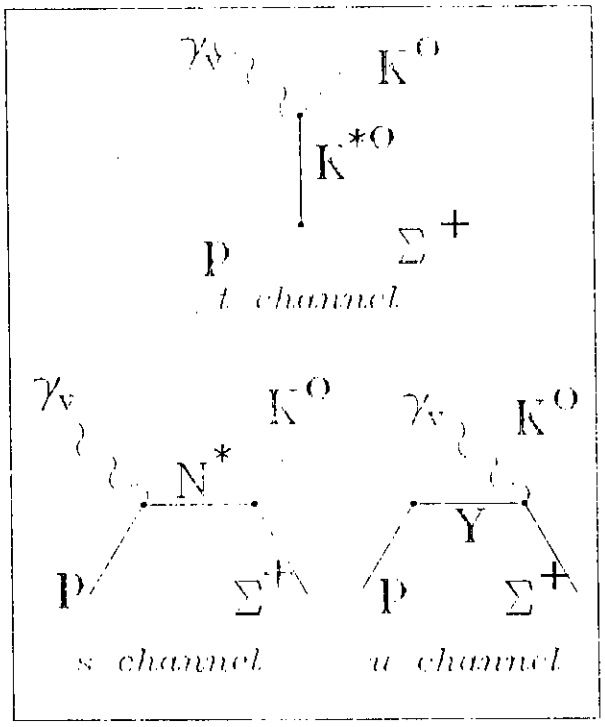

Fig. 3. Feynman diagrams in the hadrodynamic models.

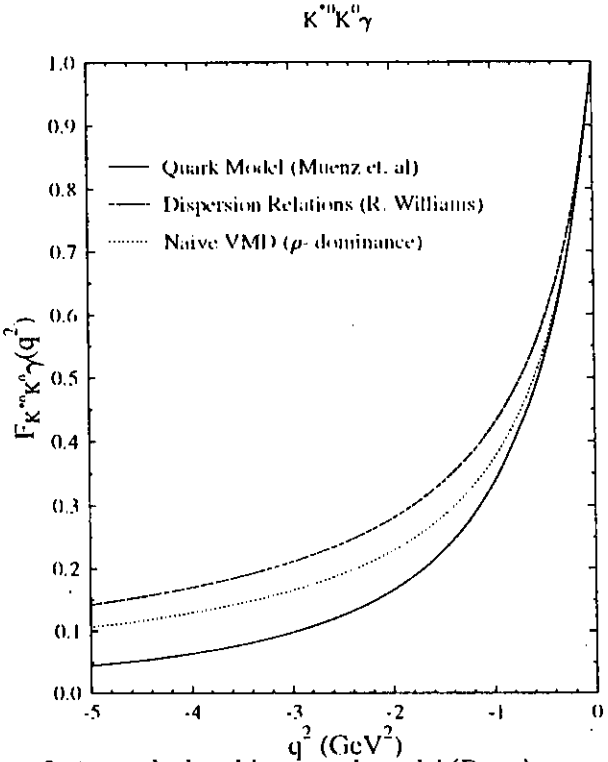

Fig. 4. Kaon transition form factors calculated in a quark model (Bonn), a model based on dispersion relations, and a naive vector meson dominance (VMD).

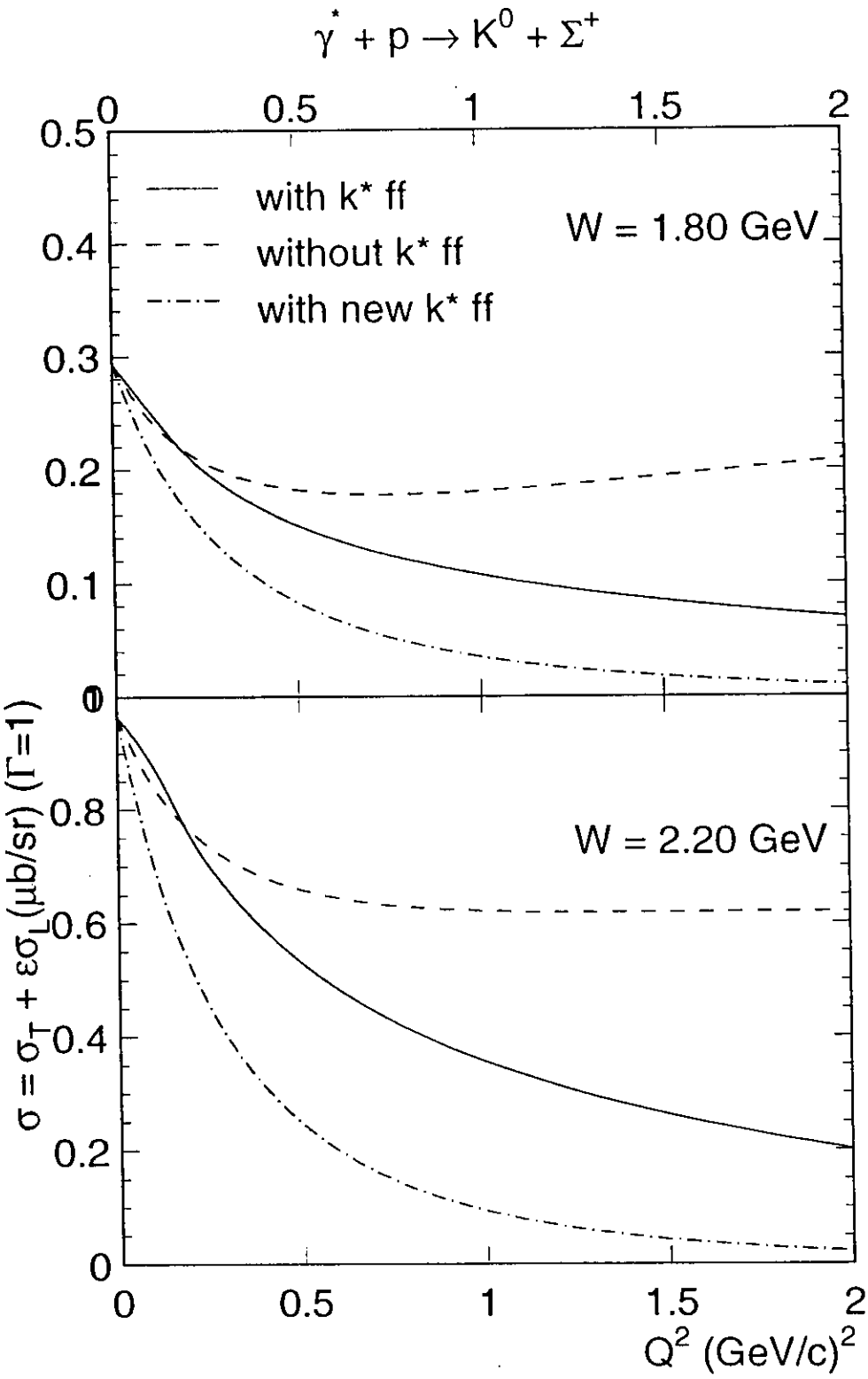

Fig. 5. Cross section calculation, comparing effect of transition form factors from Bonn quark model and vector meson dominance.

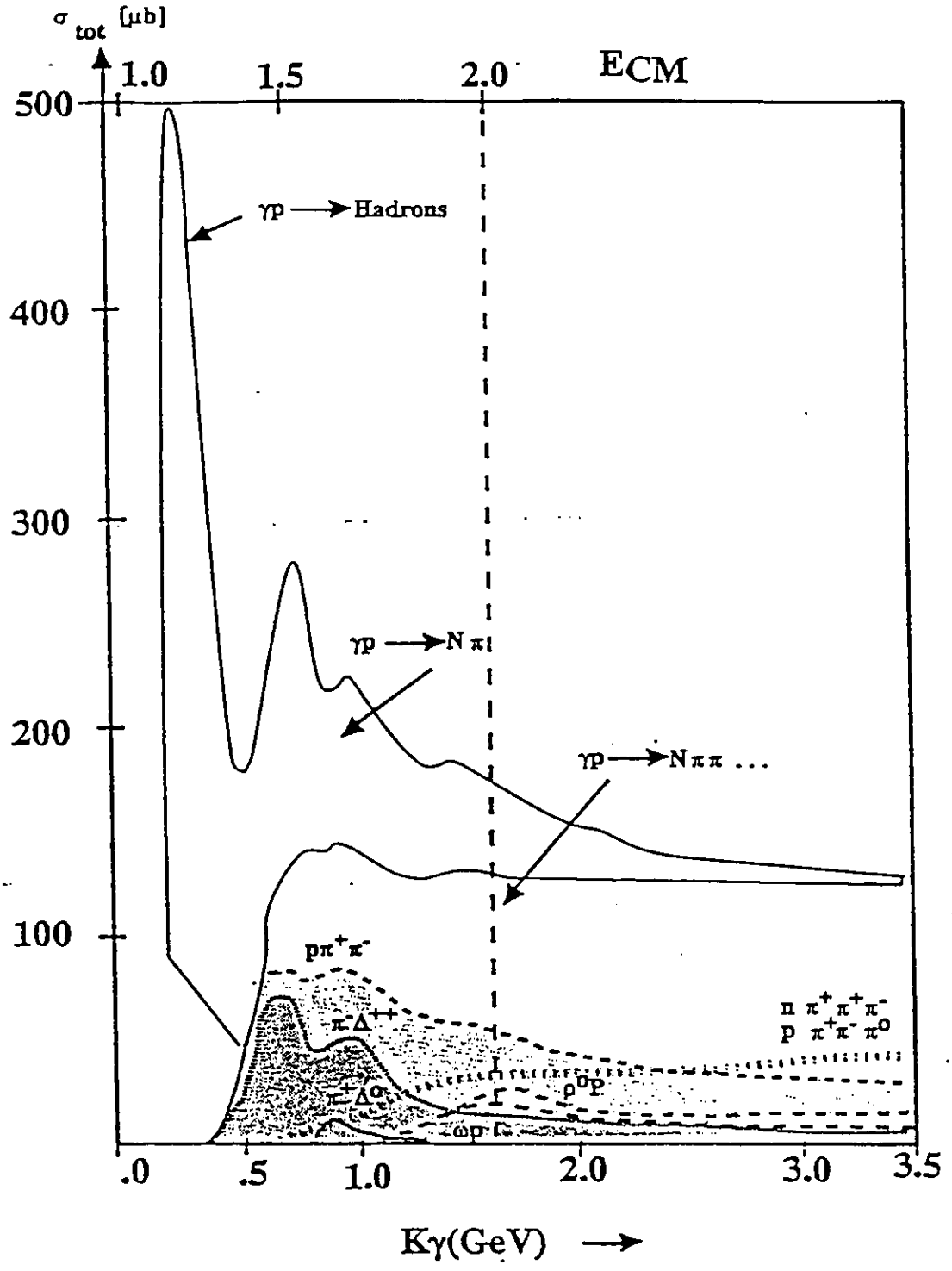

FIG. 6. Cross sections for multipion production.

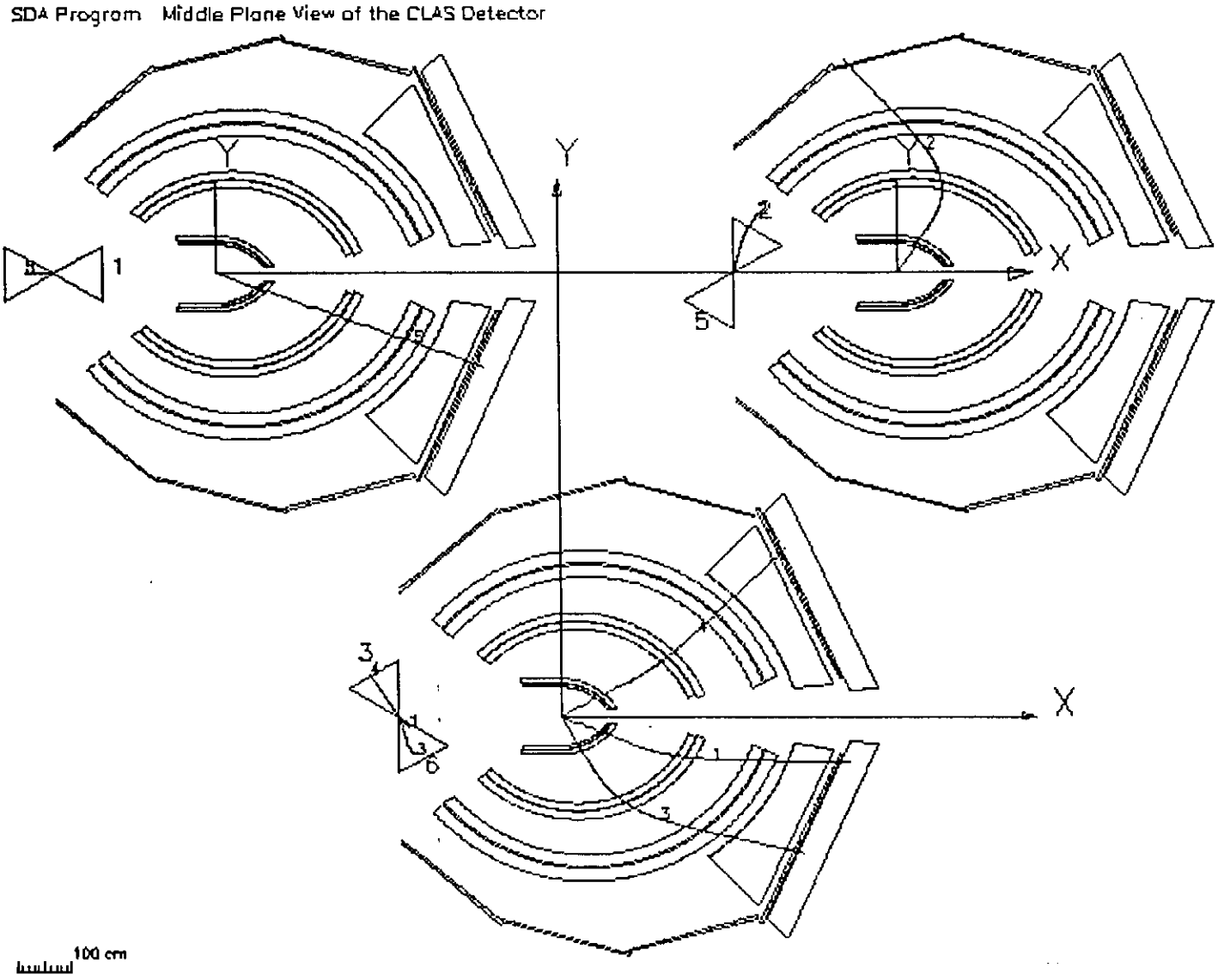

Fig. 7. Simulated event, showing $e + p \rightarrow e\pi^+\pi^- p\pi^\circ$.

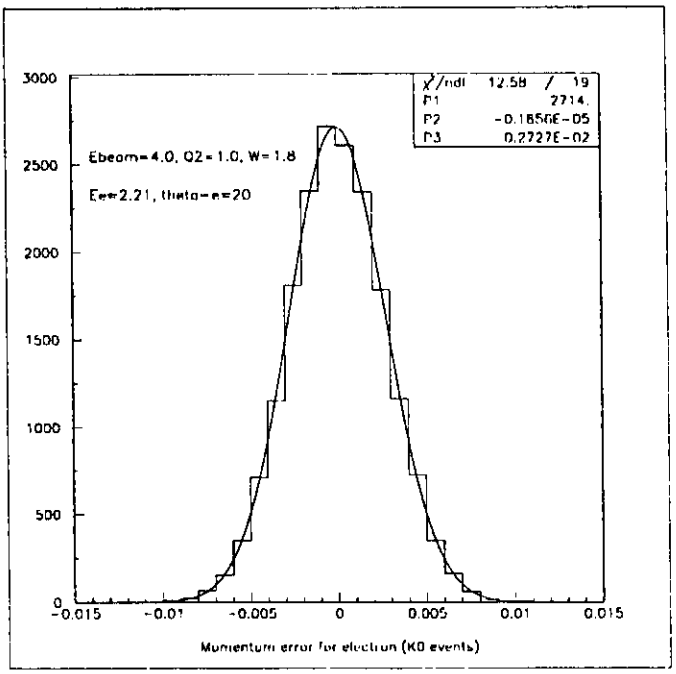

Fig. 8. Fractional momentum resolution simulated by FASTMC, scattered electrons.

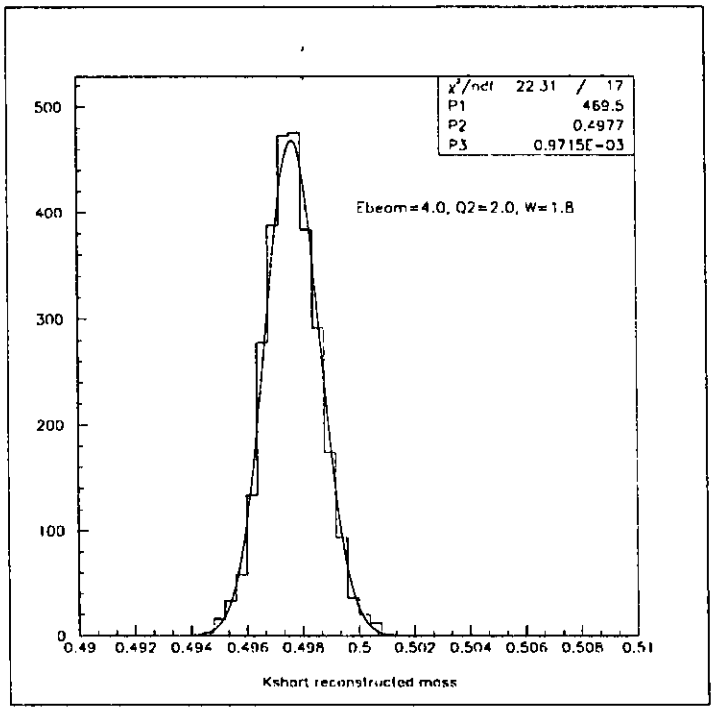

Fig. 9. Invariant mass of simulated $\pi^+\pi^-$ pairs. Additional smearing associated with tracking of the detached pion tracks or with noise hits in the drift chambers has not been included.

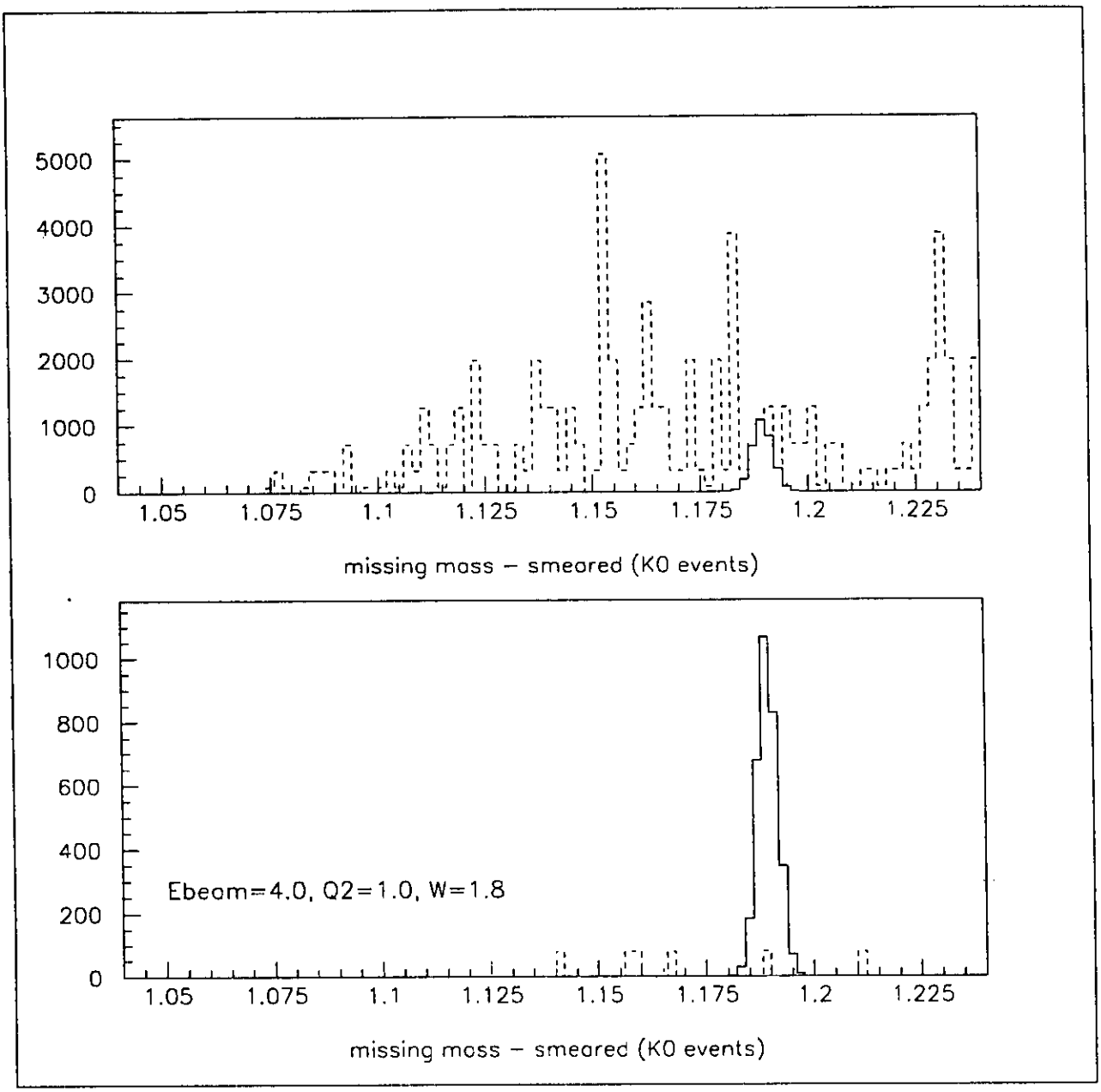

Fig. 10. a. Missing mass of events satisfying the $e\pi^+\pi^-$ acceptance criteria. Solid line is for simulated K^0_S events, dotted line for nonresonant multipion background. b. The same distributions, after a cut on the $\pi\pi$ invariant mass $0.494 < m_{\pi\pi} < 0.502$ GeV/c^2.

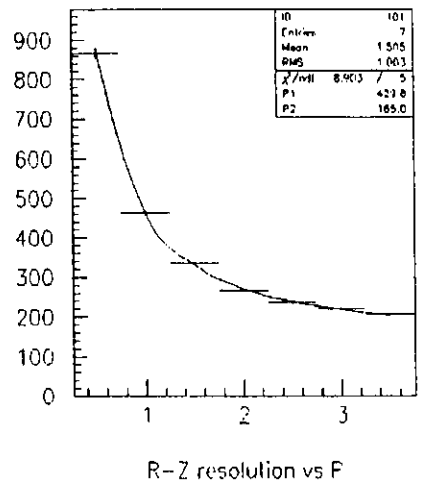

Fig. 11. Resolution of impact parameter determination (μm) as a function of pion momentum.

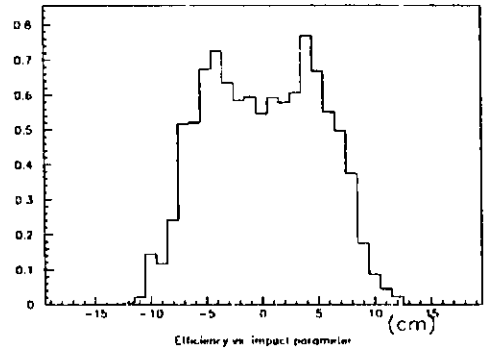

Fig. 12. Efficiency of track finding software as a function of track impact parameter.

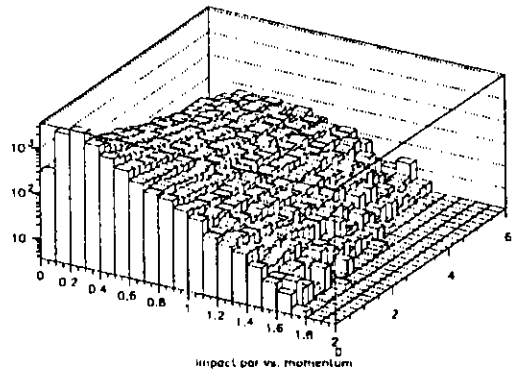

Fig. 13. Impact parameter vs. momentum for pions of K° decay. Incident 4.0 GeV/c beam.

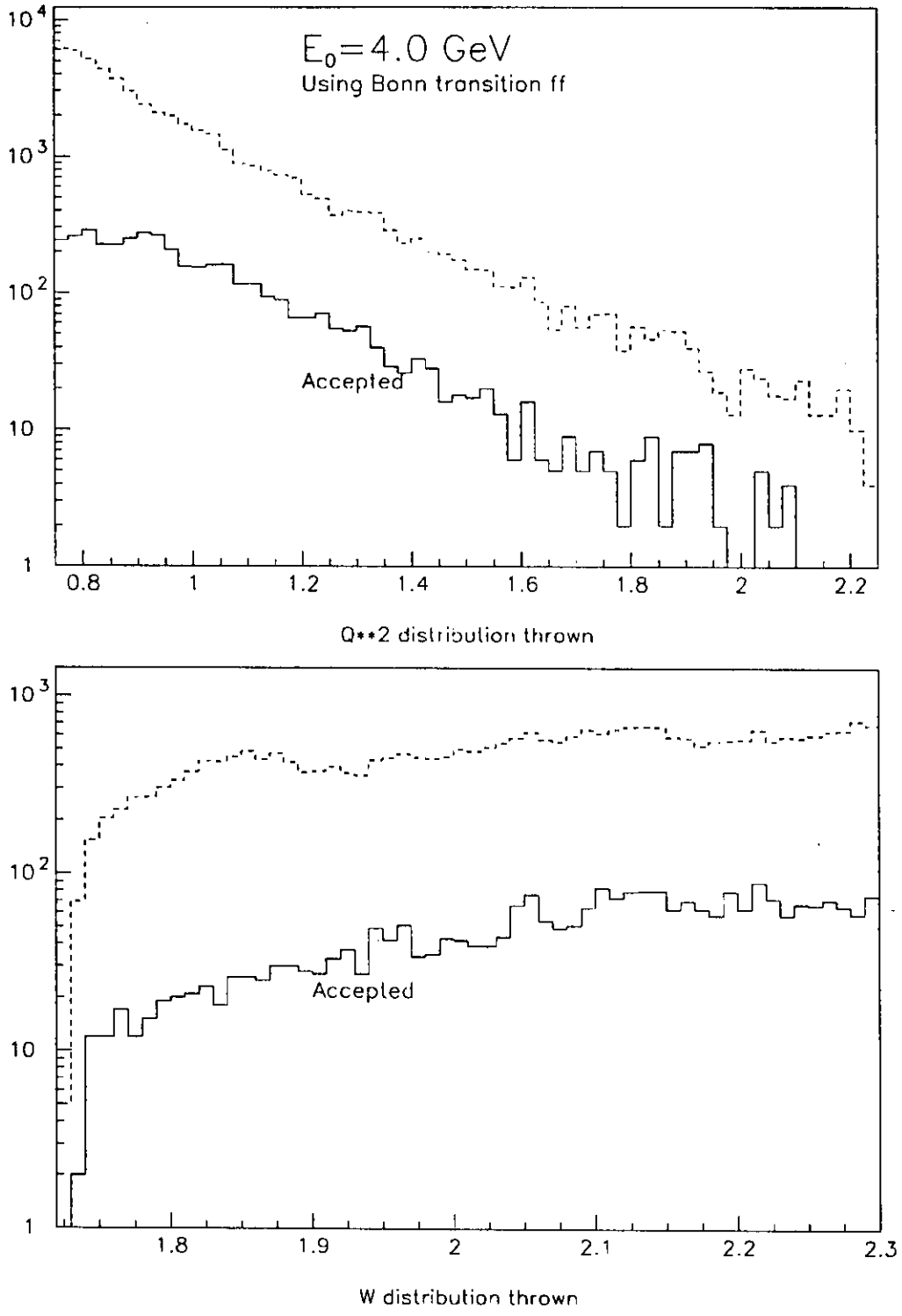

Fig. 14. Upper plot: Q^2 distribution generated by Monte Carlo (dotted) and accepted through the detector (solid). Lower plot: The same for the hadronic mass W.

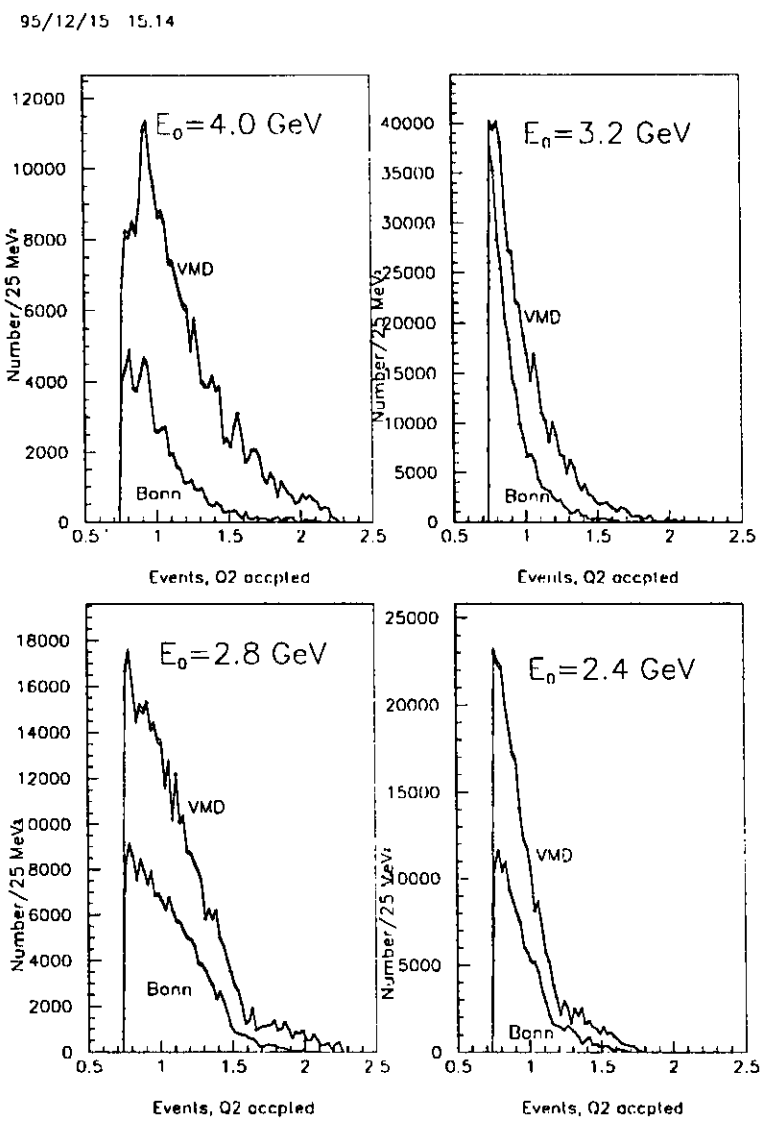

Fig. 15. Q^2 distributions expected for the four sets of running conditions. The thickness of the curves reflects the expected statistical errors, fluctuations are from finite Monte Carlo statistics.

BEAM REQUIREMENTS LIST

CEBAF Proposal No.:_____ Date: 18 Dec 95

(For CEBAF User Liaison Office use only.)

List all combinations of anticipated targets and beam conditions required to execute the experiment. (This list will form the primary basis for the Radiation Safety Assesment Document (RSAD) calculations that must be performed for each experiment.)

Condition #	Beam Energy (MeV)	Beam Current (μA)	Polarization and Other Special Requirements (e.g., time structure)	Target Material (use multiple rows for complex targets — e.g., w/windows)	Target Material Thickness (mg/cm²)
1	2400	0.1	(none)	H2 gas	5 - 20
2	2800	0.1	(none)	H2 gas	5 - 20
3	3200	0.1	(none)	H2 gas	5 - 20
4	4000	0.1	(none)	H2 gas	5 - 20
All running is concurrent with CLAS "e1" running period					

The beam energies, E_{Beam}, available are: $E_{Beam} = N \times E_{Linac}$ where N = 1, 2, 3, 4, or 5. For 1995, E_{Linac} = 800 MeV, i.e., available E_{Beam} 800, 1600, 2400, 3200, and 4000 MeV. Starting in 1996, in an evolutionary way (and not necessarily in the order given) the follov additional values of E_{Linac} will become available: E_{Linac} = 400, 500, 600, 700, 900, 1000, 1100, and 1200 MeV. The sequence timing of the available resultant energies, E_{Beam}, will be determined by physics priorities and technical capabilities.

HAZARD IDENTIFICATION CHECKLIST

CEBAF Experiment: _____ Date: 18 December 1995

Check all items for which there is an anticipated need—do not check items that are part of the CEBAF standard experiment (HRSE, HRSH, CLAS, HMS, SOS in standard configurations).

Cryogenics
- X beamline magnets
- X analysis magnets
- _____ target
- _____ drift chambers
- _____ other

Electrical Equipment
- X cryo/electrical devices
- _____ capacitor banks
- X high voltage
- _____ exposed equipment

Radioactive/Hazardous Materials
List any radioactive or hazadorous/ toxic materials planned for use:
(none)

Pressure Vessels
- _____ inside diameter
- _____ operating pressure
- _____ window material
- _____ window thickness

Flammable Gas or Liquids
(incl. target)
type: H2 gas target
flow rate: _____
capacity: 5 ml

Other Target Materials
- ___ Beryllium (Be)
- ___ Lithium (Li)
- ___ Mercury (Hg)
- ___ Lead (Pb)
- ___ Tungsten (W)
- ___ Uranium (U)
- ___ Other (list below)

Vacuum Vessels
- _____ inside diameter
- _____ operating pressure
- _____ window material
- _____ window thickness

Radioactive Sources
- _____ permanent installation
- _____ temporary use

type: _____
strength: _____

Large Mech. Structure/System
- _____ lifting devices
- _____ motion controllers
- _____ scaffolding or elevated platforms
- _____ other

Lasers
type: _____
wattage: _____
class: _____

Installation
- _____ permanent
- _____ temporary

Use
- _____ calibration
- _____ alignment

Hazardous Materials
- ___ cyanide plating materials
- ___ scintillation oil (from)
- ___ PCBs
- ___ methane
- ___ TMAE
- ___ TEA
- ___ photographic developers
- ___ other (list below)

Notes:
All running concurrent with CLAS "el" running period

LAB RESOURCES REQUIREMENTS LIST

CEBAF Proposal No.: _____ Date: 18 December 1995
(For CEBAF User Liaison Office use only.)

List below significant resources — both equipment and human — that you are requesting *from CEBAF* in support of mounting and executing the proposed experiment. Do not include items that will be routinely supplied to all running experiments, such as the base equipment for the hall and technical support for routine operation, installation, and maintenance.

***Major Installations** (either your equip. or new equip. requested from CEBAF)*

New Support Structures: _____

Data Acquisition/Reduction

Computing Resources: _____

New Software: _____

Major Equipment

Magnets _____

Power Supplies _____

Targets H2 gas

Detectors _____

Electronics _____

Computer Hardware _____

Other _____

Other

Concurrent running with CLAS

"e1" running period